LAWRENCE
LIVERMORE
NATIONAL
LABORATORY

LLNL-JRNL-656259

Impact of the Pedestal Plasma Density on Dynamics of ELM Crashes and Energy Loss Scaling

X. Q. Xu, J. F. Ma, G. Q. Li

July 1, 2014

Physics of Plasmas

Disclaimer

This document was prepared as an account of work sponsored by an agency of the United States government. Neither the United States government nor Lawrence Livermore National Security, LLC, nor any of their employees makes any warranty, expressed or implied, or assumes any legal liability or responsibility for the accuracy, completeness, or usefulness of any information, apparatus, product, or process disclosed, or represents that its use would not infringe privately owned rights. Reference herein to any specific commercial product, process, or service by trade name, trademark, manufacturer, or otherwise does not necessarily constitute or imply its endorsement, recommendation, or favoring by the United States government or Lawrence Livermore National Security, LLC. The views and opinions of authors expressed herein do not necessarily state or reflect those of the United States government or Lawrence Livermore National Security, LLC, and shall not be used for advertising or product endorsement purposes.

December 1, 2014

Impact of the Pedestal Plasma Density on Dynamics of ELM Crashes and Energy Loss Scaling*

X. Q. Xu[1], J. F. Ma[1,2], and G. Q. Li[1,3]

[1]Lawrence Livermore National Laboratory, Livermore, CA 94551

[2]Institute for Fusion Studies, University of Texas, Austin, TX 78712, USA

[3]Institute of Plasma Physics, Chinese Academy of Sciences, Hefei, China

The latest BOUT++ studies show an emerging understanding of dynamics of ELM crashes and the consistent collisionality scaling of ELM energy losses with the world multi-tokamak database. A series of BOUT++ simulations are conducted to investigate the scaling characteristics of the ELM energy losses vs collisionality via a density scan. Linear results demonstrate that as the pedestal collisionality decreases, the growth rate of the peeling-ballooning modes decreases for high n but increases for low n ($1 < n < 5$), therefore the width of the growth rate spectrum $\gamma(n)$ becomes narrower and the peak growth shifts to lower n. Nonlinear BOUT++ simulations show a two-stage process of ELM crash evolution of (i) initial bursts of pressure blob and void creation and (ii) inward void propagation. The inward void propagation stirs the top of pedestal plasma and yields an increasing ELM size with decreasing collisionality after a series of micro-bursts. The pedestal plasma density plays a major role in determining the ELM energy loss through its effect on the edge bootstrap current and ion diamagnetic stabilization. The critical trend emerges as a transition (1) linearly from ballooning-dominated states at high collisionality to peeling-dominated states at low collisionality with decreasing density; and (2) nonlinearly from turbulence spreading dynamics at high collisionality into avalanche-like dynamics at low collisionality.

*xxu@llnl.gov

The phenomena of nonlocal transport, such as avalanches or turbulence spreading, are well-known in diverse systems. Examples include, but are not limited to: piles of granular matter, discrete energy dissipating events in earthquakes and solar flares, and turbulent overshoot and penetration in fluid turbulence. Nonlocal dynamics of turbulence, transport and zonal flows are often observed in plasma turbulence simulations and experiments, such as Edge Localized Modes (ELMs) in tokamaks. ELMs are a common characteristic feature of the tokamak H-mode plasma regime, where the high frequency ELM instability repeats periodically throughout the high confinement mode (H-mode) phase of the discharge.[1] The instability causes quasi-periodic relaxations of the edge pedestal, resulting in a series of hot plasma eruptions on a fast MHD timescale and leading to large energy fluxes to the plasma facing components (PFCs), which will suffer from excessive ablation, fast erosion or melting. The concern about the survival of PFCs in ITER has sparked intense interest in ELM dynamics and in the parameter scaling of ELM energy loss. Numerous experiments in divertor tokamaks have shown a decrease in the relative Type I ELM energy loss with increasing pedestal density (collisionality) over a decade ago.[2] There are attempts to provide an explanation for the dependence of ELM energy loss on collisionality.[3] However, there is as yet no common accepted explanation of the observed scaling neither from analytical theory nor numerical simulations.[4]

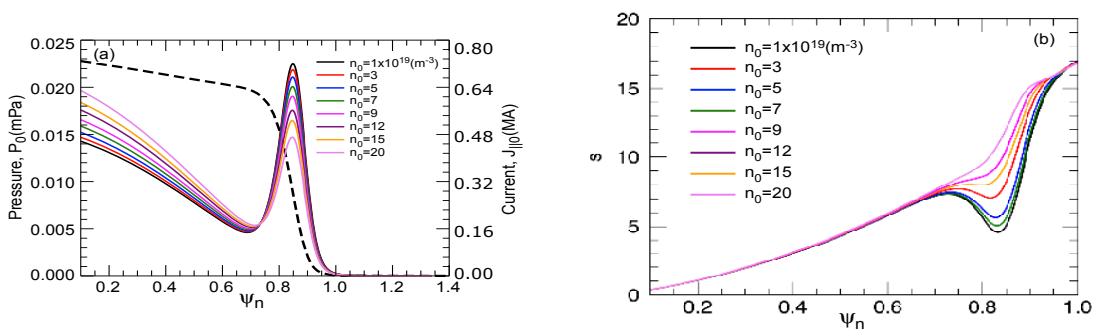

Figure 1: (Color online) (a) The radial equilibrium pressure profiles (dashed curve) and current (solid curve) for a density scan starting from an equilibrium (cbm18 dens6). (b) The radial profiles of corresponding magnetic shear s for the density scan.

Here we report on the latest BOUT++ linear and nonlinear simulations to address the important open question which physical mechanisms and parameters determine the ELM size, i.e., the ELM induced energy losses. The results illustrate the consistent collisionality scaling of ELM energy losses with experiments. At present, peeling-ballooning (P-B) theory is the leading candidate for

predicting the onset of a type-I ELM in multiple fusion devices. The theory indicates that a type-I ELM instability is triggered when an edge ideal MHD mode is destabilized as the pedestal pressure gradient exceeds its linear marginal stability limit.[5] Nonlinear BOUT++ simulations of the P-B modes show a two-stage and multi-mode process of ELM crash evolution consisting of an initial burst of pressure blob and void creation; and then inward void propagation. For initial burst, we derived a new nonlinear criterion for the occurrence of fast relaxation (crash) events at the edge of H-mode plasmas.[6] We show that for an ELM burst to occur, the coherence time of the relative phase between potential and pressure perturbations must be long enough to allow growth to large amplitude. This phase coherence time is determined by both linear and nonlinear dynamics. After initial burst, the inward void propagation stirs the top of pedestal plasma and yields an increasing ELM size with decreasing collisionality after a series of micro-bursts, giving even larger additional relative pedestal energy loss, which is in reasonable agreement with multi-tokamak experimental data.

A number of various sophisticated nonlinear two-fluid and Gyro-Landau-Fluid physics models have been developed in BOUT++ framework to simulate ELMs in the shaped plasma geometry with x-point.[7–10] Here the simulations are carried out using a simple three-field two-fluid model described in [11]. The simulation model consists of a minimum set of nonlinear equations for perturbations of the magnetic flux $A_{\|}$, electric potential ϕ, and pressure P, which can be extracted from a complete set of BOUT two-fluids equations[12] with an additional effect of hyper-resistivity. The non-ideal physics effects include diamagnetic drift, ExB drift, resistivity, and anomalous electron viscosity. Beyond the ELM energy losses, more sophisticated plasma models are obviously required to understand experimental observations and gain insight into possible new dynamics of particle losses and the ELM energy loss for different species.[7,13]

To study the physics of nonlinear P-B mode dynamics, we choose circular cross-section toroidal equilibrium (cbm18_dens6) near the marginal P-B instability threshold, which has been simulated for H-mode plasmas with steep pressure gradient at the edge.[11] Major parameters are a minor radius $a = 1.2$m, major radius $R_0 = 3.4$m, toroidal field on axis $B_0 = 2T$, the pedestal pressure 2/3 of the axis pressure, and a pedestal pressure half width 7% of the poloidal flux. In previous study,[11] edge density $n_0 = 1\times10^{19}m^{-3}$ is treated as a constant in space-time across simulation domain. Here in order to study the impact of bootstrap current on the P-B modes via magnetic equilibrium, we carefully partition the pressure between density and temperature as their gradients independently

go into the bootstrap current drive. For given density profile, we back out the temperature from the pressure profile, assuming that electron and ion temperature are equal $T_e = T_i$. As it turns out, this is a crucial step in getting the consistent collisionality scaling of ELM energy losses with the world multi-tokamak database, which is missing in previous work.[3,7,8]

We examine seven cases with increasing central density $n_0 = 1, 3, 5, 7, 9, 12, 20\times10^{19} m^{-3}$, $n_{e0}(\psi) = n_0(P_0(\psi)/P_0(0))^{0.3}$, and $T_{e0}(\psi) = P_0/2n_{e0}(\psi)$. For each density n_0, the magnetic equilibrium is reproduced with the TEQ equilibrium module in CORSICA code,[14] while keeping the plasma cross-sectional shape, total stored energy, total plasma current, pressure, the radial location of the top of the pedestal density and temperature, the ratio of the density gradient scale length to the temperature scale length profiles fixed. The neoclassical collisionality ν^* at peak gradient position increases by a factor of 3262 from 0.0019 to 6.197. The edge current is calculated from the Sauter bootstrap current model.[15] The radial profiles of pressure and current are shown in Fig. 1(a) over the range of normalized poloidal flux ψ_n ($0.1 < \psi_n < 1.4$). For the same pressure profile, but different partitions between density and temperature, pedestal bootstrap currents changes dramatically. As the pedestal density (collisionality) decreases by a factor of 20, increasing peak pedestal bootstrap currents about 50% reduce the pedestal magnetic shear about a factor of 2, as shown in Fig. 1(b). With this approach, we are able to obtain a realistic evaluation of the ELM energy loss scaling with increasing pedestal density because all cases should have the same relative distance to the stability boundary in a $(j_\parallel - \alpha)$ diagram or the same maximum growth rates of the peeling-ballooning (P-B) modes.

The radial simulation domain is ψ_n=[0.1, 1.4]. The definition of the plasma edge is somewhat arbitrary since here there is no "real" scrape-off-layer, and so $\psi_n = 1$ is defined as the point where the equilibrium plasma pressure gradient and parallel current fall to zero. In the present simplified model, both equilibrium flow and turbulent zonal flow have been assumed to be zero: $\mathbf{V}_0 = \mathbf{V}_{E0} + \mathbf{V}_{\nabla P_i} = 0$ and $\langle \delta\mathbf{v}\rangle_\zeta = \langle \mathbf{v}_E\rangle_\zeta + \langle \mathbf{v}_{\nabla P_i}\rangle_\zeta = 0$ by setting $\langle \varpi\rangle_\zeta = 0$. Therefore, both equilibrium and turbulent $E \times B$ flow are tied to diamagnetic flow. This implies that the Er well collapse results from the loss of pedestal pressure during the collapse phase of the ELM. In addition, we use typical pedestal Lundquist number $S = 10^8$ and the hyper-Lundquist number $S_H = 10^{15}$. For linear low-n ideal MHD modes, good agreement has been found between BOUT++ and GATO results.[16]

For various densities n_0 with pressure profile fixed, the linear simulations in Fig. 2 show that

as the edge density (collisionality) varies, the maximum growth rates of the peeling-ballooning (P-B) modes are almost the same, but the shape of the growth rate spectrum $\gamma(n)$ changes rather dramatically. As the pedestal collisionality decreases, the growth rate of the P-B mode decreases for high n but increases for low n ($1 < n < 5$), therefore the width of the growth rate spectrum $\gamma(n)$ becomes narrower and the peak growth shifts to lower n as shown in Fig. 2(a). The reason is that the bootstrap current plays a complex dual role in the pedestal. On the one hand, increasing currents drive peeling instabilities at low n, while at the same time the increasing pedestal current increases the local magnetic shear, which stabilizes high-n ballooning modes.[16] For the fixed pressure profile, the ion diamagnetic drift is inversely proportional to density, when density decreases, the ion diamagnetic stabilization dominates over the magnetic shear stabilization. Fig. 2(b) shows the comparison of the ion diamagnetic stabilization (square) vs. magnetic shear stabilization (diamond) of the instability growth rate over toroidal mode spectrum for $n_0 = 1 \times 10^{19} m^{-3}$. In short, the maximum growth rates of the peeling-ballooning (P-B) modes are determined by the pressure gradient, but the shape of the growth rate spectrum $\gamma(n)$ is determined by density via ion diamagnetic stabilization and bootstrap current. The consistent features of linear P-B modes are found in both shifted circular geometry and DIII-D x-point divertor geometry.

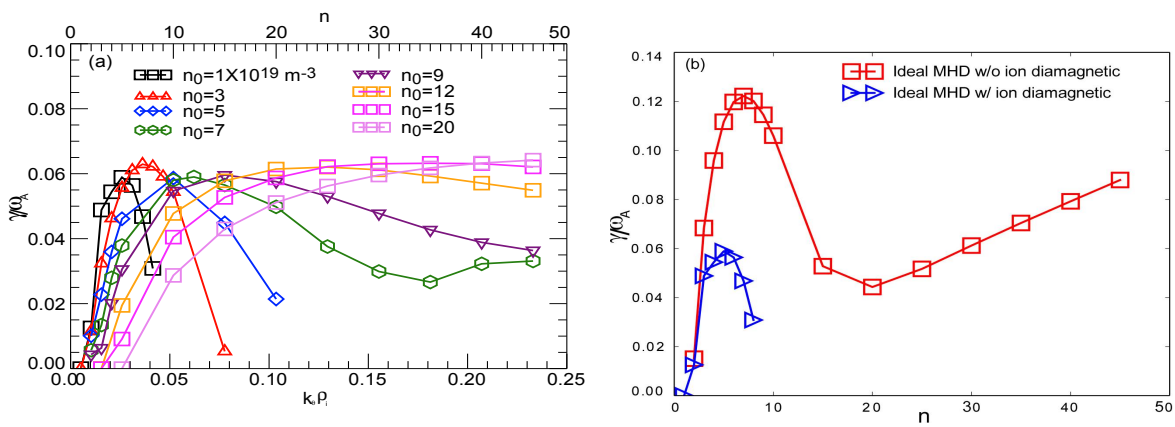

Figure 2: (a) Toroidal mode spectrum of the instability growth rate calculated by BOUT++ for the density scan. The growth rates are normalized to the Alfvén frequency ω_A. (b) Toroidal mode spectrum of the instability growth rate for comparison of the ion diamagnetic stabilization (square) vs. magnetic shear stabilization (diamond).

The nonlinear simulations are initialized with a set of small random pressure fluctuations. The fastest growing modes dominate the initial phase of the calculation, in which the P-B modes grow at their respective exponential rates. After this initial linear growing phase, the P-B modes trigger

magnetic reconnection, which drives the collapse of the pedestal pressure and creates pressure blobs and voids, and then follows by the slow inward avalanches and/or turbulence spreading, depending on collisionality. For the case with low density $n_0 = 3 \times 10^{19} m^{-3}$, Fig. 3(a) shows the profile evolution of the flux-averaged pressure perturbation $\langle \delta P \rangle_{\zeta,\theta}$ at the outer mid-plane for several different time slices, which are normalized separately to their respective absolute maximum. The respective normalized maximum are $\langle \delta P \rangle_{\zeta,\theta}^{max} = (0.29, 5.04, 4.35, 4.51, 4.62, 4.93) \times 10^{-3}$ for $t = (120, 200, 400, 600, 900, 1300)\tau_A$, respectively. Here $\tau_A \simeq 0.34\mu s$ for all cases. The dashed curve is the rms-value of linear pressure perturbation at outside midplane, which has a shape of Gaussian pulse peaking at the largest equilibrium pressure gradient location. It is clearly shown that the pedestal pressure collapses deeply inside the pedestal plasmas. The flux-averaged pressure perturbation $\langle \delta P \rangle_{\zeta,\theta}$ after the initial crash has a shape of the first derivative of a Gaussian pulse with zero crossing at the largest equilibrium pressure gradient position (defining the outer radial pivot point), positive side representing pressure blobs and negative side representing the voids for the lowest toroidal and poloidal mode numbers ($n = m = 0$), which greatly flattens the total pressure profile ($\langle P \rangle_{\zeta,\theta} = P_0 + \langle \delta P \rangle_{\zeta,\theta}$), with the pedestal pressure collapsing and the SOL pressure increasing. The radial extent of the initial collapse at $t = 120\tau_A$ is comparable to the width of linear P-B modes. After the initial crash, the overall shape of the flux-averaged pressure perturbation $\langle \delta P \rangle_{\zeta,\theta}$ is preserved near the pivot point and even their respective absolute maximum remains with some fluctuations. However, inner edge of the first derivative of a Gaussian pulse (voids) propagates inward and outer edge of that (blobs) propagates outward until the perturbation reaches the boundaries. For the case with low density $n_0 = 3 \times 10^{19} m^{-3}$, the inward propagation is due to local unstable P-B modes moving inward as the local steepening pressure profile moves inward following a series of micro-collapses, which leads to a fast avalanche dynamics. For higher density, the inward propagation is due to transport of turbulence energy from unstable peak gradient region into stable region on the top of pedestal as local P-B modes remain stable there during the inward-propagating phase.

We demonstrate that two important factors determine the size of ELMs: (1) linear growth rate and (2) nonlinear growth time. The linear growth rate is determined by linear models of plasma physics and magnetic equilibrium configurations. While the growth time of linear drives is determined by nonlinear process via phase evolution, either background turbulence and/or the spectrum of linear unstable modes.. The phase coherence time (PCT, τ_c^n) is the length of time

duration of the relative phase between pressure and potential perturbation of nth toroidal Fourier component for linear growth.[6] In linear theory, since there is no mode interaction, an unstable mode has infinitely long PCT, i.e., $\tau_c^n \to \infty$. In nonlinear theory and simulations, the growth of any unstable mode will be interrupted by nonlinear process via phase scattering. Therefore the mode amplitude depends on wave-wave interaction. For a given time at $t = 1000\tau_A$ during the inward propagation phase, Fig. 3(b) shows the flux-averaged pressure perturbation $\langle \delta P \rangle_{\zeta,\theta}(t)$ for several different densities at the outer mid-plane, which are normalized separately to their respective absolute maximum. The respective normalized maximum are $\langle \delta P \rangle_{\zeta,\theta}^{max} = (4.8, 4.4, 4.1) \times 10^{-3}$ for $n_0 = (3, 7, 12) \times 10^{19} m^{-3}$, respectively. The lower density leads to larger initial crash. As shown in Fig. 2, as the edge density (collisionality) varies, the maximum growth rates of the peeling-ballooning (P-B) modes are almost the same with linear drives fixed, but the shape of the growth rate spectrum $\gamma(n)$ changes rather dramatically. As the pedestal collisionality decreases, the growth rate of the P-B mode decreases for high n but increases for low n ($1 < n < 5$), and the width of the growth rate spectrum $\gamma(n)$ becomes narrower and the peak growth shifts to lower n. For the same background turbulence, the narrow mode spectrum leads to weak nonlinear phase scattering, which in turn leads to Long PCT. Therefore for low density, the most unstable mode will be able to grow to large amplitude, which leads to an large ELM.

The rms-profiles of linear pressure perturbation at outside midplane are also shown as shape of Gaussian pulse peaking at the largest equilibrium pressure gradient position and their widths are comparable separately to those of their respective width of linear P-B modes. This indicates that the ELM affected region is wider than both the steep gradient region and the linear eigenmode width. These simulation results lead to an important conclusion that the reduction of ELM energy loss with increasing density (or collisionality) is not accompanied by a reduction of the volume affected by the ELMs but by a decrease of the perturbation to the pressure caused by the ELM in an approximately constant volume. This is in agreement with experimental observations.[2,4,17]

To investigate the ELM energy loss scaling with density, the difference between the pre-ELM and post-ELM pressure profiles can be integrated to determine the ELM energy lost at an ELM. We define an ELM size or ELM loss fraction as $\Delta_{ELM} = \Delta W_{PED}/W_{PED} = \langle \int_{\psi_{in}}^{\psi_{out}} d\psi \oint J d\theta d\zeta \, (P_0 - \langle P \rangle_\zeta) \rangle_t / \int_{\psi_{in}}^{\psi_{out}} d\psi \oint J d\theta d\zeta$, the ratio of the ELM energy loss (ΔW_{PED}) to the pedestal stored energy W_{ped}, the ELM size can be calculated from each nonlinear simulation. Here P_0 is the pre-ELM pedestal pressure, P is the pedestal pressure during an ELM event and

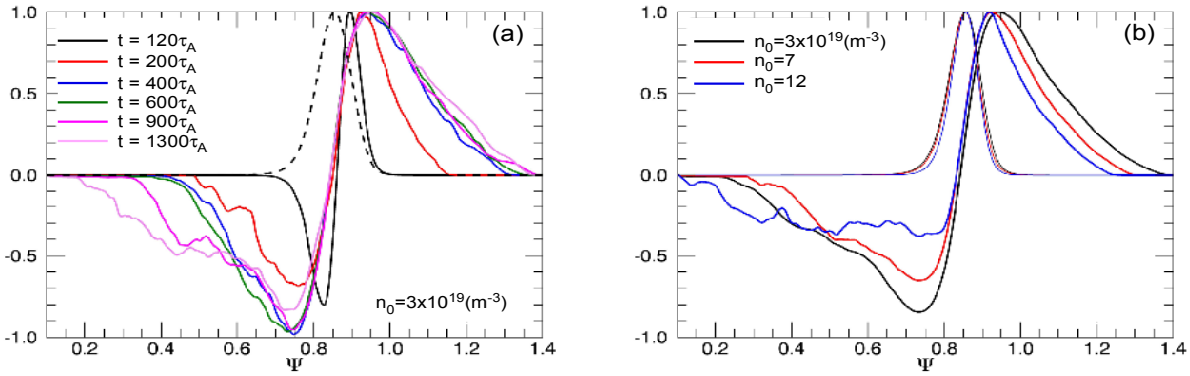

Figure 3: (a) Profile evolution of surface-averaged pressure perturbation $\langle \delta P \rangle_{\zeta,\theta}$ at different times during an ELM event and inward propagation for $n_0 = 3 \times 10^{19} m^{-3}$; (b) Profile of surface-averaged pressure perturbation $\langle \delta P \rangle_{\zeta,\theta}$ at $t = 1000\tau_A$ for different density $n_0 = 3, 7, 9 \times 10^{19} m^{-3}$. Here $\tau_A \simeq 0.34 \mu s$ for all cases.

symbol $\langle \rangle_\zeta$ means the average over bi-normal periodic coordinate. The lower integral limit is the pedestal inner radial boundary ψ_{in}, while the upper limit is the pivot point ψ_{out} (the radial position of the peak pressure gradient), J is the Jacobian.

Figure 4(a) shows the time history of the ELM energy loss fraction Δ_{ELM} for the density scan (solid curve). It is clearly shown three stages of an ELM event: (1) a linear growing phase from $t \simeq 0$ to $100\tau_A$; (2) a fast crash phase from $t \simeq 100\tau_A$ to $200\tau_A$ to $500\tau_A$, depending on the density, and (3) following by a slow inward propagation phase until the perturbation eventually reaches the boundaries. The energy lost at an ELM inward propagation phase can be two to three times larger than its initial fast crash phase. The lower density (low collisionality) leads to fast inward-propagating ELM, which reach inner boundary sooner and lead to a sharply increased energy loss, as shown in Fig. 4(a) for $n_0 = 3 \times 10^{19} m^{-3}$ at $t \simeq 1200\tau_A$ and for $n_0 = 5 \times 10^{19} m^{-3}$ at $t \simeq 2500\tau_A$. On this transport time scale, it is expected that heating flux from core finally balances the ELM energy loss and the ELM is terminated. The pedestal profiles rebuild, so long as the heating power is maintained. Therefore, the exact ELM energy loss fraction also depends on heating power and/or level of gas fueling, which will determine the pressure affected depth and the beginning of of the recovery phase. In order to investigate possible inward-propagating mechanisms without additional complication of introducing sources, the dashed lines are introduced for linear extrapolation of the ELM energy loss (ΔW_{PED}) for these cases as if the system were infinite large to remove boundary effects. It is shown that ELM energy loss fraction increases during inward propagation and decreases

with increasing density during both the crash phase and late in inward-propagating phase.

To compare these scaling trends with experimental data, we pick up the the ELM energy loss fraction at the late ELM inward-propagating phase, such as $t \simeq 4500\tau_A = 1.5$ms (indicated by vertical dashed line). The data are plotted in Fig. 4(b) with the trends from the world multi-tokamak experimental data overlaid.[2] Although BOUT++ simulations have been performed using a set of circular cross-section toroidal equilibria, the ELM size reduction with increasing pedestal plasma collisionality is in reasonable agreement for a large range of Type-I ELMy H-mode plasmas in tokamaks, such as ASDEX Upgrade, DIII-D, JT-60U and JET including various plasma triangularities, ratios of P_{INPUT}/P_{L-H} and pellet triggered ELMs. It is clearly shown that the pedestal plasma density plays a major role in determining the ELM energy loss through its effect on the edge bootstrap current and ion diamagnetic stabilization. Other parameters such as the plasma shape, pedestal heights and widths, edge flow shear, heating level and feedback of evolving bootstrap currents after pedestal collapses, etc, possibly play additional role in determining the ELM energy loss, and are likely needed for comparisons with particular experiments.

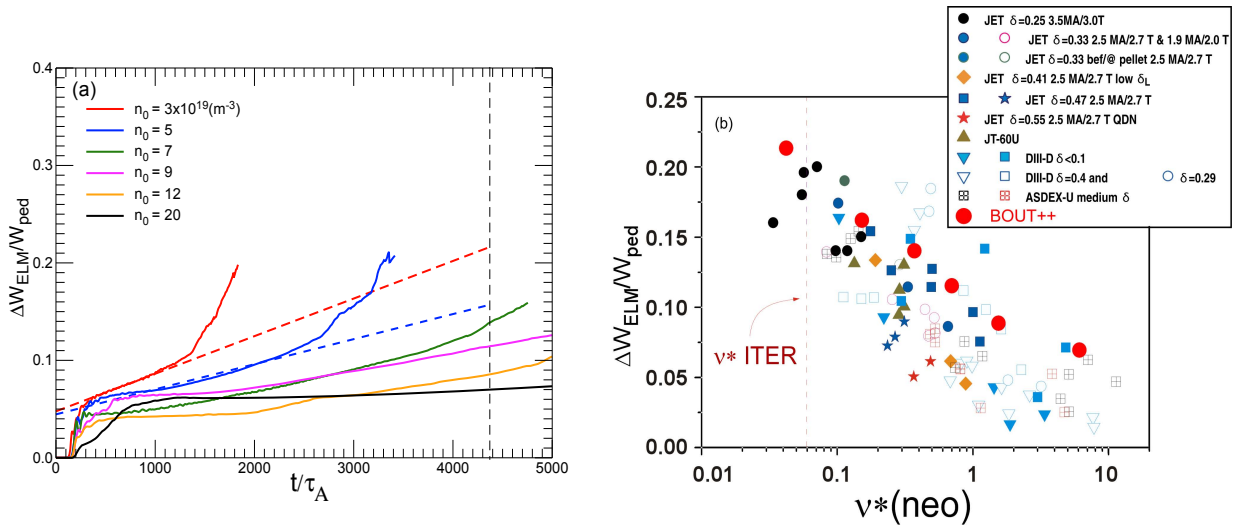

Figure 4: (a) The time history of the plasma ELM loss fraction ($\Delta W_{ped}/W_{ped}$) (solid curve) for the density scan; (b) The relative ELM energy loss scaling vs. collisionality is plotted with multi-tokamak experimental data[2] overlaid with BOUT++ simulation results (red bullet),

In conclusion, the simple three-field two-fluid model is found good enough to simulate pedestal collapse and the ELM energy loss scaling with density. The pedestal plasma density plays a major role in determining the ELM energy loss scaling through its effect on the edge bootstrap current

and ion diamagnetic stabilization. The bootstrap current plays dual roles on the P-B modes via magnetic equilibrium to increase the local magnetic shear and to increase peeling drive. The critical trend emerges as a transition from ballooning-dominated states at high collisionality to peeling-dominated states at low collisionality with decreasing density.

After the initial linear exponential growing phase, the P-B modes trigger magnetic reconnection, which drives the collapse of the pedestal pressure and creates pressure blobs and voids. The inward void propagation stirs the top of pedestal plasma and yields an increasing ELM size with decreasing density (collisionality). As the edge density (collisionality) decreases, the unstable mode spectrum shifts to lower n, initial bursts increase in intensity, and nonlocal transport undergoes a dynamic transition from turbulence spreading at high collisionality into avalanches at low collisionality. This leads to larger relative pedestal energy loss during an ELM evolution. The inward-propagating rate due to turbulent transport increases as the edge density decreases, giving even larger additional relative pedestal energy loss. The relative ELM energy loss scaling vs. collisionality is in reasonable agreement with multi-tokamak experimental data.

ACKNOWLEDGMENTS This work was performed under the auspices of the U.S. Department of Energy by Lawrence Livermore National Laboratory under Contract DE-AC52-07NA27344 and by IFS-UT Austin under Contract DE-FG02-04ER-54742. This material is based upon work supported by the U.S. Department of Energy, Office of Science, Office of Fusion Energy Sciences. LLNL LDRD project 12-ERD-022 and LDRD project 11-ERD-058, and the China Natural Science Foundation under Contract No.10721505. The authors wish to thank Drs. B. Dudson, M. V. Umansky, P. B. Snyder, H. Wilson, A. W. Leonard, A. Kirk, and A. Loarte, G. T. A. Huijsmans, P. H. Diamond, F. Waelbroeck and T. Y. Xia, and Mr. C. H. Ma and Mr. P. W. Xi for useful discussions. LLNL-JRNL-656259.

References

[1]H. Zohm, Plasma Phys. Controlled Fusion 38, 1213 (1996).

[2]A. Loarte, G. Saibene, and R. Sartori, D. Campbell, M. Becoulet, L. Horton, T. Eich, A. Herrmann, G. Matthews, N. Asakura, A. Chankin, A. Leonard, G. Porter, G. Federici, G. Janeschitz, M. Shimada and M. Sugihara, Plasma Phys. Controlled Fusion 45, 1549 (2003).

[3]G. T. A. Huysmans, et al, 2010 Proc. 23rd Int. Conf. on Fusion Energy 2010 (Daejeon, Korea, 2010) paper TH7-1, www-naweb.iaea.org/napc/physics/FEC/FEC2010/index.htm

[4]A. W. Leonard, Phys. Plasmas 21, 090501 (2014).

[5]P. B. Snyder, H. R. Wilson, J. R. Ferron, L. L. Lao, A. W Leonard, T. H Osborne, A. D. Turnbull, D. Mossessian, M. Murakami, and X. Q. Xu, Phys. Plasmas 9, 2037 (2002).

[6]P. W. Xi, X. Q. Xu, and P. H. Diamond, Phys. Rev. Lett. 112, 085001 (2014).

[7]X. Q. Xu, P. W. Xi, A. Dimits, I. Joseph, M. V. Umansky, T. Y. Xia, B. Gui, S. S. Kim, G. Y. Park, T. Rhee, H. Jhang, P. H. Diamond, B. Dudson, and P. B. Snyder, Physics of Plasmas 20, 056113 (2013).

[8]T. Y. Xia, X. Q. Xu and P. W. Xi, Nucl. Fusion 53 2013 073009.

[9]C. H. Ma,, X. Q. Xu, P. W. Xi, T. Y. Xia, P. B. Snyder, and S. S. Kim, submitted to Phys. Plasmas (2014)

[10]B. D. Dudson, M. V. Umansky, X. Q. Xu, P. B. Snyder, and H. R. Wilson, Comput. Phys. Comm., 180,1467 (2009).

[11]X. Q. Xu, B. Dudson, P. B. Snyder, M. V. Umansky, and H. Wilson, Phys. Rev. Lett. **105**, 175005 (2010).

[12]X. Q. Xu, R. H. Cohen, T. D. Rognlien, and J. R. Myra, Physics of Plasma 7, 1951-1958 (2000); X. Q. Xu, M. V. Umansky, B. Dudson and P. B. Snyder, Comm. in Comput. Phys. 4, 949(2008).

[13]C. H. Ma, X. Q. Xu, P. W. Xi, and T. Y.Xia, submitted to Phys. Plasmas. (2014)

[14]J. A. Crotinger, L. LoDestro, L. D. Pearlstein, A. Tarditi, T. A. Casper, and E. B. Hooper, LLNL Report UCRL ID-126284, NTIS #PB2005-102154 (1997).

[15]O. Sauter, C. Angioni, and Y. R. Lin-Liu, Phys. Plasmas 9, 5140 (2002); O. Sauter, C. Angioni, and Y. Lin-Liu, Phys. Plasmas 6, 2834 (1999).

[16]G. Q. Li, X. Q. Xu, P. B. Snyder, A. D. Turnbull, T. Y. Xia1, C. H. Ma, P. W. Xi, Phys. of Plasmas 21, 102511 (2014).

[17]I. Nunes, G. D. Conway, A. Loarte, M. Manso, F. Serra, W. Suttrop and the CFN and ASDEX Upgrade teams, Nucl. Fusion 44 883 (2004).